PAPER

Check for updates

Boosting the activity of UiO-66(Zr) by defect engineering: efficient aldol condensation of furfural and MIBK for the production of bio jet-fuel precursors†

María Sanz, [ID] [a] Pedro Leo, [ID] [a] Carlos Palomino, [ID] [b] Marta Paniagua, [ID] [a] Gabriel Morales [ID] [a,c] and Juan A. Melero [ID] *[a,c]

The production of jet-fuel precursors from furfural *via* aldol-condensation with methyl-isobutyl ketone (MIBK) over defect-engineered UiO-66(Zr) catalysts is presented. The catalysts are prepared using formic acid (FA), trifluoroacetic acid (TFA) and HCl as synthesis modulators, leading to the incorporation of defects on the microcrystalline structure of the metalorganic framework (MOF) material, which dramatically boosts the catalytic performance. An extensive characterization of the modified catalysts by means of X-ray diffraction (XRD), argon adsorption isotherm, thermogravimetry (TGA), transmission electron microscopy, and FTIR spectroscopy of adsorbed acetonitrile, confirmed the incorporation of missing-linker and missing-node defects within the MOF structure, enabling the explanation of the enhancement in the catalytic process. The analysis of the reaction kinetics evidences that, working under moderate temperature conditions, conversion of furfural and selectivity to the desired adduct (FuMe) close to 100% can be achieved, avoiding the formation of degradation and bulkier compounds. Finally, despite the generation of defects within the UiO-66(Zr) structure, the resultant catalyst displays good reusability in low furfural concentration mediums.

1. Introduction

Global climate emergency and diminishing fossil fuels are stimulating the development of sustainable resources to replace the current oil-based economy. In particular, decarbonizing the transportation sector, accounting for over 25% of the greenhouse gases emissions, is critical to reach the ambitious global climate objectives. The fast-growing aviation sector is especially sensitive to this problem. Advanced biofuels, representing biofuels produced from inedible renewable feedstock, are among the alternatives contemplated for introducing sustainable energy in the hard-to-electrify airborne transport.[1,2] In this sense, lignocellulosic materials, which constitute the most important and massive biomass resource, are being intensively

*aChemical and Environmental Engineering Group, ESCET,
Universidad Rey Juan Carlos, c/Tulipán s/n, 28933 Móstoles, Spain.
E-mail: juan.melero@urjc.es; Tel: +34-91 665 50 83*
*bDepartment of Chemistry, University of the Balearic Islands, Cra. de Valldemossa,
07122, Spain*
*cInstituto de Investigación de Tecnologías para la Sostenibilidad, ESCET,
Universidad Rey Juan Carlos, c/Tulipán s/n, 28933 Móstoles, Spain*
†Electronic supplementary information (ESI) available. See DOI: https://doi.org/
10.1039/d3gc05022j

promoted.[3–8] Despite its chemical complexity and high oxygen content, lignocellulose is a highly versatile raw material that can be employed to prepare promising platform chemicals such as furfural.[9,10] Furfural (FAL), already a common industrial solvent used as extraction agent for the refining of lubricating oils, may also find use as a precursor for manufacturing an extensive portfolio of chemicals and oxygenated and drop-in biofuels (such as gasoline, diesel, or jet fuel-range hydrocarbons).[11,12]

Lignocellulosic bio-jet fuel can be synthesized starting from renewable platform chemicals like FAL by C–C coupling reactions and subsequent hydrodeoxygenation/hydrogenation.[13,14] C–C coupling reactions include alkylation,[15] aldol condensation,[16] oligomerization,[17] Michael reaction,[18] and Diels–Alder reaction.[19] Among them, aldol condensation is one of the most frequently explored routes for the synthesis of bio-jet fuel from FAL due to the availability of biomass-derived ketone substrates, the relatively moderate reaction conditions, and the possibility of being catalyzed either by acids or bases. The aldol condensation of FAL to fuel precursors has been widely explored in the last decade, mainly focusing on the use of acetone as reacting ketone.[20–32] However, the small size of acetone limits its applicability for the production of jet-fuel range fuel components. Thus, in recent studies the use of

larger, cyclic or branched ketones, like cyclopentanone[28,30,32,33] and methyl isobutyl ketone (MIBK)[34,35] has been explored.

Solid base catalysts such as Ca- and Mg-based oxides, La- and Zn-based catalysts, have been proposed for the aldol condensation of FAL as an environmentally friendly alternative to the use of homogeneous bases.[20–22,31,36] However, in this type of base catalysts, poor stability issues typically result in significant leaching of the active species. In contrast, Brønsted acid catalysts (e.g., sulfonic acid-based resins, acid zeolites) have shown low selectivity towards the desired condensation adducts due to the formation of undesired polymeric by-products.[32] Lewis acid zeolites have also been explored in the condensation of FAL with acetone, leading to higher selectivities.[23,24] On the other hand, metal–organic frameworks (MOFs) are gaining increasing interest as heterogeneous catalysts,[37,38] particularly for biomass transformations.[39,40] In this field, current research is focused on the use of MOF materials displaying enhanced resistance properties, able to overcome the typical low stability of MOFs in reaction media. Thus, some zirconium-based MOFs feature exceptional thermal, chemical, and mechanical stabilities.[41,42] Among them, UiO-66(Zr) has received considerable attention due to high stability and an easy and reproducible lab-scale preparation.[43] Standard UiO-66(Zr) is composed of an inner $Zr_6O_4(OH)_4$ core in which the triangular faces of the Zr_6-octahedron are capped by μ_3-O and μ_3-OH groups, wherein the connection among zirconium oxo-clusters is made through organic ligands, usually benzen-1,4-dicarboxilate (BDC) moieties. In this way, one secondary building unit (SBU) of UiO-66 is coordinated by 12 Zr_6 clusters via 12 BDC linkers. Because of this high connectivity and elevated degree of coordination, the structural integrity can be well maintained after linker or even Zr cluster removal. Furthermore, the high oxidation state of Zr(IV) is also key to the stability, both in organic solvents and water.

On the other hand, UiO-66(Zr) is amenable of tailoring through defect engineering, bringing about beneficial changes to the catalytic properties.[44] Indeed, the inherent stability of UiO-66(Zr) materials allows for the introduction of a relatively high level of defects without impairing its crystalline structure and physical properties. Up to date, several parameters have been studied for the defect engineering of UiO-66(Zr) during the synthesis: temperature and Zr/linker ratio,[45] selection of Zr precursor,[46] thermal activation,[47] linker modification,[48] metal cation substitution,[49] and addition of synthesis modulators.[50,51] In catalytic terms, defects introduced in UiO-66(Zr) not only change the pore structure, but also entail beneficial changes in its catalytic abilities. Thus, improved performance can be achieved when defective UiO-66(Zr) is used as Lewis and/or Brønsted acids.[52,53]

In this context, we have recently reported the aldol condensation of biomass-derived FAL and MIBK over a defective Zr-based UiO-66 MOF prepared using formic acid as modulator.[54] Acetone is a byproduct in the manufacture of bio-butanol and bio-ethanol via the ABE (acetone, butanol, and ethanol) fermentation of lignocellulose which can be further converted to MIBK via self-aldol condensation followed by selective hydrogenation.[55] The use of this carboxylic acid as modulator during the synthesis allowed to incorporate both missing-linker and missing-node defects within the MOF structure, increasing the mean pore size and the accessibility to the Zr and μ_3-OH catalytically active species. As a result, the modified UiO-66(Zr) MOF displayed a superior catalytic performance as compared to other solid acid catalysts. In a step forward, within this work we present a systematic analysis on the use of different known modulators, i.e., formic acid, trifluoroacetic acid, and hydrochloric acid, at different concentrations during the synthesis of UiO-66(Zr). Microscopic characterization of the series of prepared materials through powder XRD, Ar adsorption–desorption isotherms, thermogravimetric analysis, transmission electron microscopy, and FTIR spectroscopy of adsorbed CD_3CN, is correlated to the catalytic behavior in the production of bio-jet fuel precursors via aldol condensation of FAL and MIBK. This manuscript describes a very significant improvement in catalyst performance via modulation with acids.

2. Experimental

2.1 Catalysts preparation

Defect-free UiO-66(Zr) material, without noticeable defects in its structure (herein denoted as UiO-66(Zr)-DF), was synthesized as described by Shearer et al. with a 2 : 1 BDC : Zr molar ratio and a synthesis temperature of 220 °C.[56] These conditions shift the solution equilibrium in favour of BDC–Zr bonds, minimizing the formation of structural defects. The synthesis was performed by sequential addition of 3.78 g of $ZrCl_4$ (16.2 mmol, Merck, 98%), 2.86 ml of 35 wt% HCl (32.4 mmol), and 91.9 g of N,N′-dimethyl formamide (DMF, Quimipur, 99.8%). After obtaining a homogeneous solution (stirring 60 min), 5.39 g of benzen-1,4-dicarboxilate, BDC (32.4 mmol, Merck, 98%), was added under stirring (180 min). The resultant mixture was hydrothermally aged at 220 °C for 20 h in a Teflon-lined stainless-steel autoclave. Centrifugation in DMF (3×), and methanol (3×) allows for the recovery and washing of the precipitated solid, which was subsequently dried overnight at 80 °C. Finally, the material was thermally-activated for 16 h at 150 °C.

Modulated UiO-66(Zr) series of materials were prepared adapting the procedure described by Cliffe et al. for the incorporation of Zr instead of Hf.[57] Typically, 1.4 g of $ZrCl_4$ (6 mmol) was dissolved in the corresponding mixture of modulator and DMF (Table ESI-1†). In order to tune the generation of defects, different molar ratios modulator/DMF and different modulators were tested in the present work: formic acid (FA, Merck, 96%), trifluoroacetic acid (TFA, Merck, 99%), and aqueous hydrochloric acid (HCl, Merck, 35 wt%). After obtaining a homogeneous solution (60 min), 1 g of BDC (6 mmol) was added under stirring (60 min). The resultant mixture was hydrothermally aged at 120 °C for 48 h in a Schott Duran pressure bottle. Centrifugation in DMF (3×), and methanol

(3×) allows for the recovery and washing of the precipitated solid, which was subsequently dried overnight at 80 °C and thermally-activated for 16 h at 150 °C. Sample nomenclature includes the initials for the modulator species followed by a consecutive integer, in order of growing modulator/DMF molar ratio. The composition in the synthesis media for each material is shown in Table ESI-1.† The synthesis of the parent UiO-66(Zr) was carried out following the same solvothermal synthesis described for modulated UiO-66(Zr) series, but without addition of any modulator.

2.2   Catalyst characterization

The textural properties of the synthesized MOFs were determined from Ar adsorption–desorption isotherms, recorded at 87 K, using a Micromeritics 3Flex Adsorption Analyzer. Surface area values were calculated using the BET method, while the pore volume was taken at $P/P_o = 0.95$ as a single point. Non-Local Density Functional Theory (NLDFT) model was applied to calculate the pore size distributions from the adsorption branch of the argon isotherm, assuming the adsorption of Ar within cylindrical pores. Crystallinity characterization was performed by X-ray powder diffraction (XRD) employing a Philips X-pert MPD diffractometer (Cu Kα radiation) and recording data in the range 5–50° of 2θ angle, with 0.02° step size and 10 s counting time. Thermogravimetric analyses (TGA) were carried out in a Mettler-Toledo SDT 2960 Simultaneous DSC-TGA Star System device with an airflow of 100 ml min^{-1} and heating ramp of 5 °C min^{-1} up to 700 °C. The acidity of the samples was investigated by CD_3CN adsorption at room temperature followed by FTIR spectroscopy using a Bruker Vertex 80v spectrophotometer working at 3 cm^{-1} resolution. Commonly, a self-supporting wafer of MOF was prepared and degassed inside an IR cell under dynamic vacuum at 403 K for 8 h. Structural characterization of the UiO-66(Zr)-HCl series of materials was completed by transmission electron microscopy (TEM) on a JEOL 1400 Flash electronic microscope operating at 120 kV. All the images are TEM BF (Bright Field).

2.3   Catalytic tests

The catalytic runs of aldol condensation of methyl isobutyl ketone (MIBK, Merck, 99.5%) and furfural (FAL, Merck, 99%) were performed in a carousel 12 Plus Reaction Station equipped with glass tubes (20 ml), with continuous stirring (400 rpm), and with temperature control by a hotplate. Prior to testing, all the catalysts were activated at 150 °C for 24 h. Reaction conditions for the catalyst's comparison were fixed as follows: MIBK/FAL molar ratio of 4/1; FAL/Cat mass ratio of 10/1; reaction temperature of 130 °C; reaction time of 4 h. Sulfolane (Merck, 99%) was added to the reaction media as internal standard, in a sulfolane/FAL molar ratio of 1/10. The kinetic evaluation reactions were carried out at different temperatures in the range 110–170 °C, and reaction times, from 0.5 to 24 h. Reusability experiments were performed after applying a mild washing procedure with acetone at room temperature to remove the reaction media remaining within the spent cata-

lyst. The resultant recovered material was then dried at 110 °C and used in a new otherwise equivalent reaction run.

2.4   Products analysis

Reaction samples were analysed by means of GC in an Agilent 7820A Gas Chromatograph, equipped with a FID detector and a high-polarity Agilent CP-WAX 52 CB column (ID 0.25 mm, film thickness 0.25 μm, length 30 m). Chemical compounds detected by GC included unreacted FAL and MIBK, sulfolane used as internal standard, and the condensation product coming from the reaction of 1 molecule of FAL with 1 molecule of MIBK, herein denoted as FuMe (Scheme 1). Noteworthy, because of the relatively mild reaction conditions used for the present catalyst screening, the higher condensation product of FuMe with a second molecule of MIBK, Fu(Me)$_2$, was not detected in the screening of materials.[54] Some unidentified compounds could be observed in the chromatograms, attributed to the formation of soluble humins, but mostly in negligible quantity. However, during the kinetics study, where more severe conditions are explored, the presence of Fu(Me)$_2$ can be identified.

A standard stock solution of commercial FAL was used to calibrate its quantification by GC. In the case of the adduct FuMe, which is commercially non-available, it was synthesised using CaO as catalyst and isolated via rotatory evaporation according to the procedure described by Pholjaroen et al.[22] Catalytic results are shown as conversion of furfural (X_{FAL}) or yield/selectivity to the desired condensation adduct (FuMe) shown in Scheme 1 (Y_{FuMe}/S_{FuMe} respectively):

$$X_{FAL} = \frac{(\text{initial mmol of FAL}) - (\text{final mmol of FAL})}{\text{initial mmol of FAL}} \times 100 \quad (1)$$

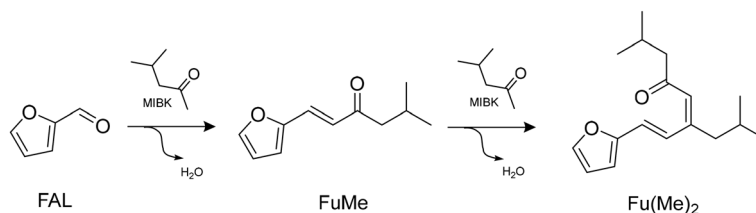$$Y_{FuMe} = \frac{\text{mmol of product FuMe}}{\text{initial mmol of FAL}} \times 100 \quad (2)$$

$$S_{FuMe} = \frac{Y_{FuMe}}{X_{FAL}} \times 100 \quad (3)$$

3.   Results and discussion

3.1   Structural characterization of modulated UiO-66(Zr)

In order to boost the activity of UiO-66(Zr) in the aldol condensation of furfural (FAL) and methyl isobutyl ketone (MIBK) for the production of bio jet-fuel precursors, the introduction of defects in the UiO-66 structure has been studied in this work. However, increasing the concentration of structural defects may lead to a detrimental outcome in terms of stability, and therefore it is necessary to further explore this phenomenon to find the adequate compromise between the preservation of the MOF structure and the enhancement of catalytic properties. The use of modulators during the synthesis involves the simultaneous incorporation of two kind of defects, missing-linker and missing-cluster defects, as they bind the metal nodes in a reversible and competitive way with regards to the structural ligand. Thus, it is important to tune the amount of modulator

Scheme 1 Aldol condensation of FAL and MIBK and main condensation products: FuMe and Fu(Me)$_2$.

used during the synthesis, on the one hand to achieve the pursued benefits in terms of catalytic performance, and on the other extreme to avoid the inhibition of the MOF crystallization.[58]

In this work, a series of modulated UiO-66(Zr) materials has been synthesized. Two kinds of modulators have been used: (i) coordination modulators: monocarboxylic acids that compete with the organic ligand (BDC) for group coordination, slowing the precipitation rate and leading to a larger crystal growth, such as formic acid, and trifluoroacetic acid; (ii) protonation modulators: strong inorganic acids, typically HCl, which slows the rate of precipitation by inhibiting the dissociation of H$_2$BDC into BDC. In order to check the structure of the synthesized materials and elucidate the type and concentration of the generated defects, the following characterization techniques were used: XRD, Ar adsorption isotherms, and TGA. Table 1 shows the main physicochemical properties of the series of modulated UiO-66(Zr) materials.

The XRD diffractograms corresponding to the reference materials, UiO-66(Zr)-DF and the parent UiO-66(Zr), together with the different series of modulated UiO-66(Zr) samples, are shown in Fig. ESI-1.† As it can be observed, the main diffrac-

tion peaks present in the defect-free UiO-66(Zr)-DF are still maintained for the materials synthesized with all the modulators and concentrations, as the patterns show very little differences in shape and intensity of the corresponding signals. These results evidence that the overall crystalline structure of the materials remains fairly unaltered even in the presence of structural defects.

Fig. 1 shows the thermogravimetric analysis of the modulated UiO-66(Zr) series of materials, including the non-modulated materials, UiO-66(Zr)-DF and UiO-66(Zr), for comparison. TGA data have been normalized to the residual ZrO$_2$ in order to quantify the level of defects. In this way, for all the samples the end weight (at 650 °C) has been assigned to 100% baseline, and in the theoretical defect-free structure a plateau at 220% corresponding to the molecular formula Zr$_6$O$_6$(BDC)$_6$ should appear in the range 360–400 °C.[58,59] As can be seen in the figure, the experimental TGA plateau of UiO-66(Zr)-DF closely matches that predicted by theory, represented by the horizontal dashed line at 220%, which confirms the high crystallinity and low level of deficiencies of this sample. For the rest of the materials, different weight losses are observed depending on temperature:[58–60] (i) release of solvent/water adsorbed in the range 50–100 °C; (ii) dehydration of the Zr$_6$O$_4$(OH)$_4$ nodes to Zr$_6$O$_6$ together with the removal of the corresponding species as a function of the modulator used during the synthesis, formate for UiO-66(Zr)-FA series,[59] trifluoroacetate for UiO-66(Zr)-TFA series,[59] and chloride groups for UiO-66(Zr)-HCl series.[61] These weight losses take place in the temperature between 200–400 °C; (iii) complete combustion of the organic BDC linkers leading to a framework decomposition in the temperature range 450–550 °C. As described in literature, the lower the mass loss at this last stage, the greater the number of defects incorporated during the synthesis of the material,[59] which matches with the amount of modulator used for the three series of UiO-66(Zr) materials synthesized. Furthermore, comparing the three modulators, HCl is the one that generates the highest number of defects since the loss of this last segment is the lowest among all the synthesized materials. It is important to note that relying only on this analysis is impossible to distinguish between missing-linker and missing-cluster defects, since both introduce linker deficiencies into the UiO-66 framework leading to alterations in the TGA-detected weight losses.[59]

In order to compare the materials synthesized with the different modulators the number of linker deficiencies per Zr$_6$

Table 1 Textural properties of modulated UiO-66(Zr) series of materials

Catalyst	S_{BET} [a] (m^2·g^{-1})	$S_{\mu p}$ [b] (m^2·g^{-1})	S_{EXT} [c] (m^2·g^{-1})	V_p [d] (cm^3·g^{-1})	$V_{\mu p}$ [e] (cm^3·g^{-1})
UiO-66(Zr)-DF	1110	1019	91	0.44	0.36
UiO-66(Zr)	1325	1216	108	0.53	0.42
UiO-66(Zr)-FA1	1265	1179	86	0.49	0.41
UiO-66(Zr)-FA2	1535	1430	105	0.58	0.49
UiO-66(Zr)-FA3	1612	1481	131	0.60	0.49
UiO-66(Zr)-FA4	1560	1378	182	0.61	0.46
UiO-66(Zr)-TFA1	818	682	136	0.43	0.24
UiO-66(Zr)-TFA2	1600	1379	221	0.67	0.48
UiO-66(Zr)-HCl1	1424	1311	113	0.55	0.45
UiO-66(Zr)-HCl2	1693	1542	151	0.63	0.50
UiO-66(Zr)-HCl3	1839	1655	184	0.68	0.52
UiO-66(Zr)-HCl4	1875	1603	272	0.84	0.53
UiO-66(Zr)-HCl5	1223	1054	169	0.54	0.35

[a] Total surface area calculated by the BET method from the adsorption branch of the corresponding argon isotherm. [b] Micropores area calculated with the *t*-plot method. [c] External surface area calculated with the *t*-plot method. [d] Total pore volume recorded at P/P_o = 0.95. [e] Micropore volume calculated with the *t*-plot method.
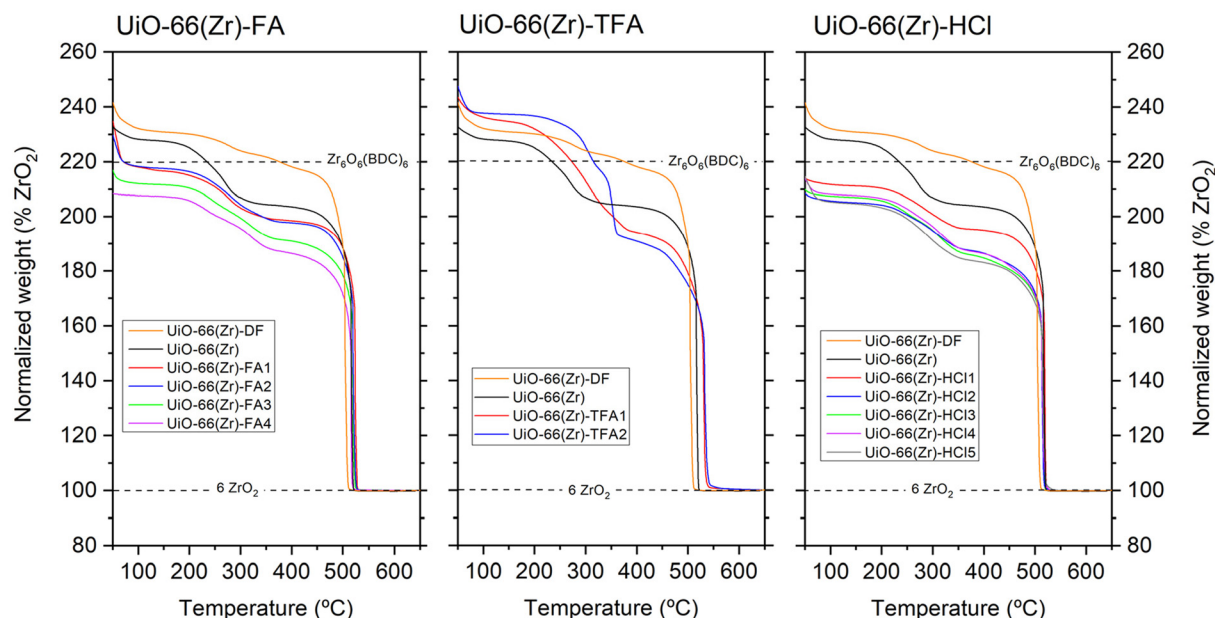
Fig. 1 Thermogravimetric analysis of UiO-66(Zr)-DF, UiO-66(Zr), and modulated UiO-66(Zr) series of materials.

formula unit has been calculated following the procedure described in literature (Table ESI-2†).[59] As the modulator/ligand molar ratio increases (Fig. ESI-2†), the number of linker deficiencies raises. Furthermore, the type of modulator used plays a very important role, since for the same modulator/ligand molar ratio the number of deficiencies generated varies significantly, achieving a higher creation of defects with the inorganic modulator HCl.

It is important to note that when a large amount of modulator is used missing-cluster defects are also expected to be formed. In those cases, the assumption of a value of 220% in the normalized data TGA in the dehydroxylated structure might not be accurate. Therefore, in order to differentiate between missing-linker and missing-cluster defects, the Ar adsorption–desorption isotherms were analyzed (Fig. ESI-3†). Argon has been used as adsorbate because of its small molecular size, unlike the typically-used N_2, as it allows for a better discrimination of the textural properties in the microporosity region. In this way, Table 1 summarizes the textural properties for the UiO-66(Zr)-DF, UiO-66(Zr) parent and modulated UiO-66(Zr) series of materials. As shown, the Ar adsorption capacity varies significantly depending on the synthesis conditions. The material with the lower surface area is the UiO-66(Zr)-DF, synthesized under specific conditions to avoid the appearance of defects. The parent UiO-66(Zr) shows a higher BET area than UiO-66(Zr)-DF, which indicates that under these synthesis conditions, equivalent to those of the modulated samples except for the absence of modulator, the structure formed already presents a certain degree of defects. On the other hand, as the amount of modulator used during the synthesis of the different series of materials systematically increases, an increase in the BET surface area is observed. The exception is UiO-66(Zr)-HCl5 material, where a decrease in the

BET area can be observed, most likely because the amount of modulator used in this sample is too high leading to an undesired worsening in the textural properties. This behavior can be attributed to a decreasing in the formation of defects due to the extremely high proton concentration in the synthesis solution which leads to a better stabilization of Zr metal clusters.[62]

Pore size distributions corresponding to modulated UiO-66(Zr) series of materials are depicted in Fig. 2. The UiO-66(Zr)-DF, without any deficiencies of linkers or clusters, only has pores with small diameters around 7 Å, in accordance with the theoretical values of the UiO-66 structure. However, the parent UiO-66(Zr), in addition to the intrinsic microporosity of the MOF structure, displays a secondary porosity at larger pore sizes, in the range 14–18 Å. Once again, this confirms that the modification of the synthesis conditions interferes with the porous structure of the material, already introducing a certain degree of defects even in the absence of modulator. Such secondary porosity can be ascribed to void generated by missing-linker defects. Looking at the series of materials synthesized with the different modulators, in general it is observed that as the amount of modulator increases, the smaller pores (first range of porosity between 5–10 Å) decrease while an increase in the secondary porosity, between 15–20 Å, occurs. The appearance of this second range of porosity can be explained by the loss of the whole Zr_6 metal cluster from the framework, as it matches with the simulated pore size distributions of UiO-66 framework with missing-cluster defects described by Shan *et al.*[62] Furthermore, it is observed how both ranges of porosity shift to higher values as the modulator concentration increases. This shift is consistent with missing-linker defects increasing the average size of the small tetrahedral pore in UiO-66.[62]
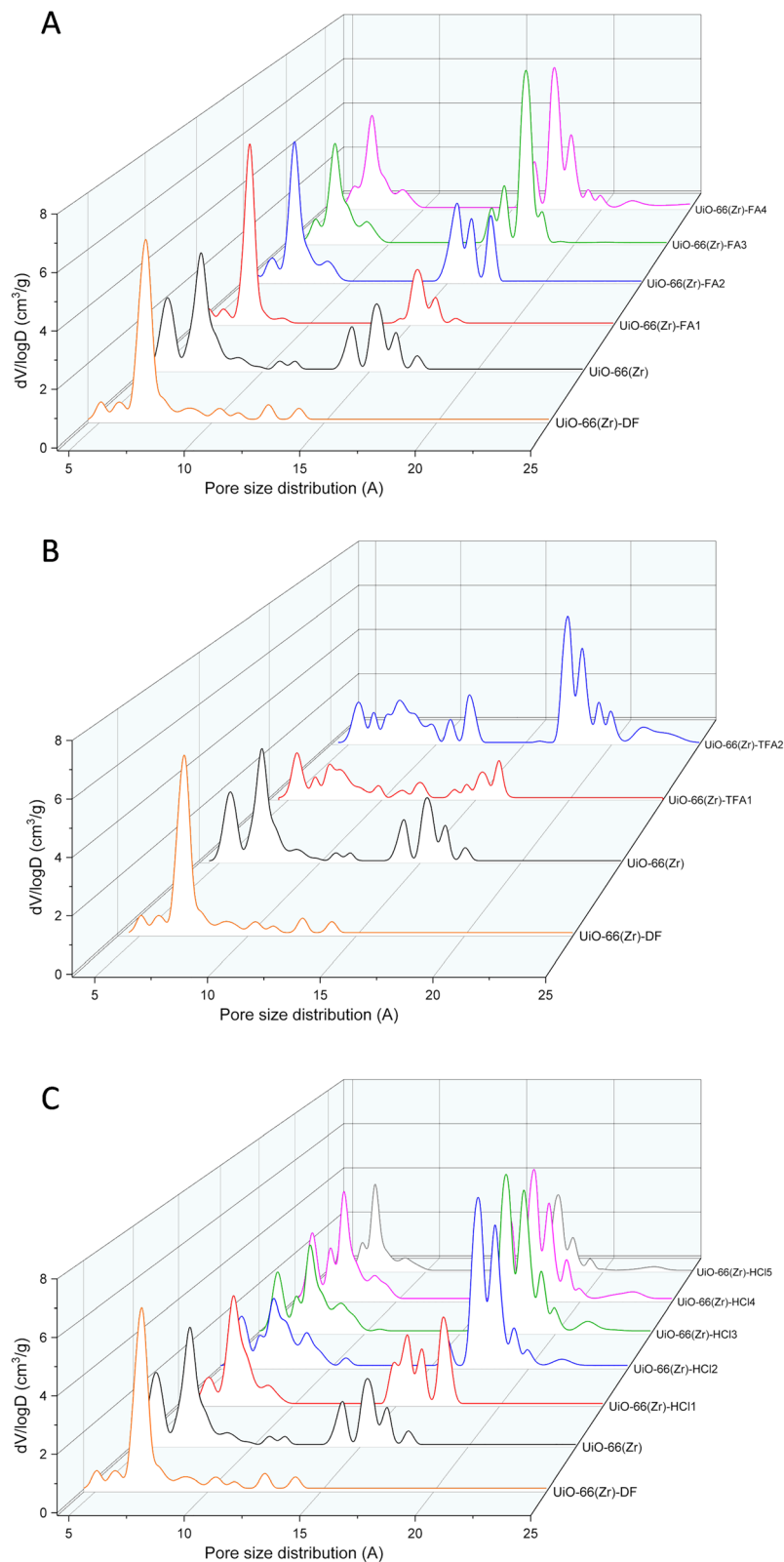
Fig. 2 Pore size distributions of modulated UiO-66(Zr) series of materials. (A) Formic acid; (B) trifluoroacetic acid; (C) hydrochloric acid.

In the case of using TFA as modulator (Fig. 2B), the disappearance of the first porosity interval is more pronounced, probably due to the larger size of that molecule, as compared to formic acid (Fig. 2A), that blocks smaller pores more easily. Finally, in the HCl series (Fig. 2C), it is observed how an excessive modulator/ligand molar ratio implies a loss in the textural properties of the material, which is reflected both in the BET surface area (Table 1) and in the porosity of the material.

In conclusion, if, in addition to modifying the synthesis conditions, a modulator is included during the synthesis process, the created defects provide a noticeable improvement in the textural properties, enlarging surface areas and pores volume as can be seen from data in Table 1.[63]

Fig. 3A and B represent the evolution of the total surface area and the total pore volume with the molar ratio modulator/ligand used in the synthesis of the different series of UiO-66 (Zr) materials. It should be noted that the synthesis of TFA-modulated samples with higher MOD/ligand molar ratios was attempted, but crystallization was totally inhibited, and the material did not form.[59] On the other hand, under FA and HCl modulation, higher MOD/ligand molar ratios were feasible and led to MOF structure formation.

The defects content is directly reflected in the BET surface area and pore volume, observing a remarkable rising with increasing MOD/ligand molar ratio, but also significant differences can be appreciated depending on the pK_a value of the organic modulator. The argon uptake of the samples increases as the pK_a of the modulator decreased, indicating that the acid strength of the modulator is an important factor in creating defects. This can be explained by the competitive cluster binding between BDC linker (pK_a value, 4.82) and modulator molecules. Modulators with lower pK_a value deprotonate easier, promoting an accumulation of H^+ in the synthesis medium, which can suppress ligand deprotonation leading to the formation of more missing-cluster defects. On the other

hand, when the pK_a of modulator and BDC linker are more similar, less defective UiO-66(Zr) is obtained.[64] Therefore, this supports that the modulator causing the highest amount of defects in the UiO-66(Zr) framework is HCl, since it has the lowest pK_a value (−6.3). In addition, the amount of HCl present in the reaction medium also affects the rate of MOF crystallization due to an enhanced solubility of precursors under low pH, leading to smaller crystal sizes and higher BET surface areas.[60] In addition, the type of defect generated in the framework is also different depending on the modulator pK_a: modulators with higher pK_a value, such as formic acid, generate more missing-linker defects while modulators with lower pK_a value, such as HCl, generate more missing-cluster defects, which have a much higher influence on increasing UiO-66(Zr) surface area and secondary porosity than the first ones.[63] Fig. 3C shows the relationship between both parameters, observing a clear linear relationship between the number of linker deficiencies, estimated by TGA, and the BET surface area. Noteworthy, the HCl-modulated materials fall within the upper right part of the graph, indicating that this modulator generates the highest number of defects, directly correlated to the highest surface areas.

3.2 Catalytic evaluation of modulated UiO-66(Zr) materials

In the previous sections it has been demonstrated that the formation of defects *via* modulated synthesis modify the textural properties of the materials. The aim of this work is to check if these changes lead also to an improvement in the catalysis, correlating the physicochemical characterization of modulated UiO-66(Zr) series with the catalytic performance. Fig. 4 shows a comprehensive comparison of the catalytic activity in the aldol condensation of FAL and MIBK of the modulated UiO-66(Zr) series of materials.

The reference non-modulated catalysts, UiO-66(Zr)-DF and parent UiO-66(Zr), show both low activity and limited selectivity to the desired FuMe adduct. In contrast, the modulated
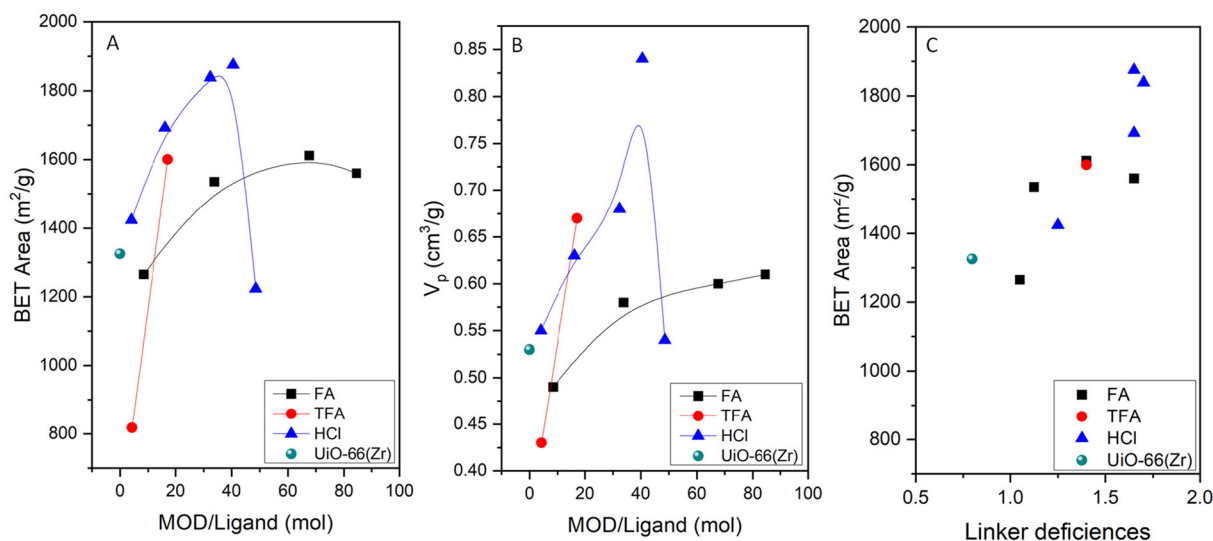

Fig. 3 Total surface area (A) and total pore volume (B) corresponding to modulated UiO-66(Zr) series of materials, as a function of MOD/ligand molar ratio, and linker deficiencies per Zr_6 unit (C).
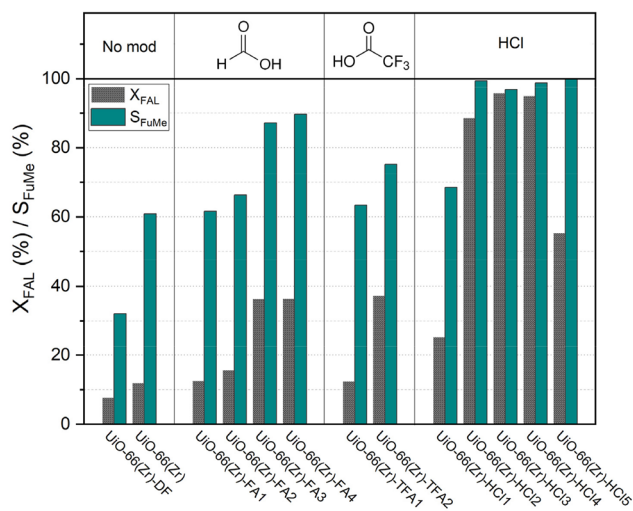
Fig. 4 Catalytic activity of the modulated UiO-66(Zr) series of materials in the aldol condensation of FAL and MIBK. Reaction conditions: time = 4 h; temperature = 130 °C; MIBK/FAL molar ratio = 4; FAL/Cat mass ratio = 10/1.

samples show significantly better results, with increasing FAL conversion and the selectivity values as the ratio MOD/ligand increases within each series of materials. This trend is in fair agreement with above-discussed enhancement of the textural properties and the generation of secondary porosity at larger pore sizes, much more adequate to allocate relatively bulky molecules like FuMe.[54]

Different trend is also observed depending on the modulator used. The best results are achieved over the HCl-modulated materials, reaching conversions over 90% combined with an almost total selectivity to FuMe. As above-discussed, the lowest pK_a of HCl seems to drive the appearance of more missing-cluster defects on the structure of the MOF material, which enhances the accessibility of reactants to the unsaturated Zr clusters within the framework by providing both larger pore sizes and surface areas. Another hypothesis would be that the increase in activity was due to a change in the coordination number of the Zr atoms. However, as said before, the overall framework structure of UiO-66(Zr) is virtually unchanged after creation of defects through modulation, as deduced from powder XRD (Figure ESI-1†), being observed for all the materials the main diffraction peaks present in the UiO-66(Zr)-DF. FA- and TFA-modulated materials, though more active and selective than the references, are far from the activity displayed by HCl-modulated samples. TFA is the bulkiest molecule among the analyzed modulators, and its use during the synthesis is expected to result in a material with partial substitution of terephthalate by trifluoroacetate moieties. Since this may have an impact on the porosity and accessibility of reactants to the active sites, in order to improve the catalytic activity of UiO-66(Zr)-TFA2 a more intensive thermal activation step was applied, 5 h at 300 °C, leading not only to the dehydroxylation of the hexanuclear Zr cluster but also to a post-synthetic removal of the anchored trifluoroacetate

groups.[61] Consequently, the resultant material (denoted as UiO-66(Zr)-TFA2-300) has a more open framework, with a larger number of open sites (Fig. ESI-4†). This thermally treated material showed an important improvement as compared to its precursor (UiO-66(Zr)-TFA2), corroborating the hypothesis of partial blocking by bulky trifluoroacetate groups, but still far away from the excellent performance of the HCl-modulated materials (Fig. ESI-5†).

On the other hand, in literature it is described that the absence of one or more organic linkers in the structure of UiO-66 results in the exposure of coordinatively unsaturated Zr atoms, creating Lewis acid sites. Also, when missing-linker defects are generated, terminal –OH groups or –OH/H_2O pairs can compensate for charge providing in this case Brønsted acid sites.[65] Hence, in order to better explain the enhancement in the catalytic aldol condensation of furfural and MIBK, the characterization of the nature of active sites by means of infrared spectroscopy with a basic molecular probe, CD_3CN, was carried out (Fig. 5), as this is the technique most used to evaluate the acid nature of this kind of materials. The IR band at 2304 cm^{-1} is associated with CD_3CN coordinated to Zr^{4+} sites,
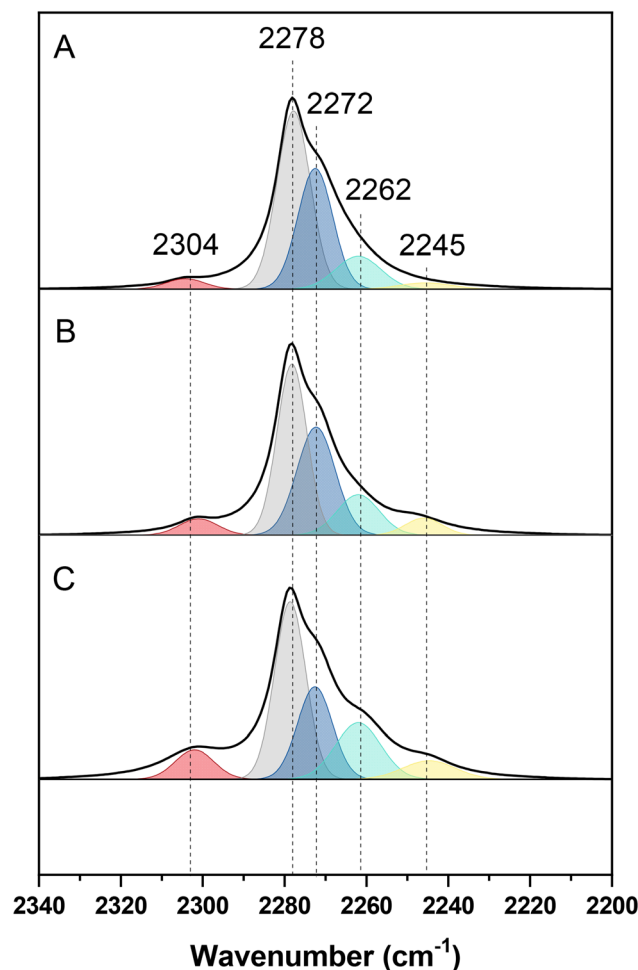

Fig. 5 FTIR spectra of CD_3CN adsorbed at room temperature of (A) UiO-66(Zr); (B) UiO-66(Zr)-HCl1; (C) UiO-66(Zr)-HCl3.

indicating the presence of Lewis acid sites. The IR bands at 2278 and 2272 cm^{-1} are attributed to medium and weak Brønsted acid sites, respectively,[66] and the IR band at 2261 cm^{-1} corresponds to physisorbed acetonitrile.[67]

As expected according to the literature, a clear increase in the amount of Lewis acid sites is observed insofar as the amount of HCl used during the synthesis of the catalysts increases, what is related to a higher generation of missing-linker defects that leads to the exposure of coordinatively unsaturated Zr atoms. This fact causes a decrease in the ratio between Brønsted and Lewis acid sites (B/L) in the following way: UiO-66(Zr) (25.3) > UiO-66(Zr)-HCl1 (14.8) > UiO-66(Zr)-HCl3 (7.8).

In conclusion, we attribute the activity to the μ_3-OH hydroxyl groups forming part of the zirconium clusters. Such hydroxyl groups are the most numerous acid groups in this kind of MOFs, being considered Brønsted in nature.[68] However, it is well known that such Brønsted acid sites can also catalyze the undesired size reactions of furfural, especially when they present high acid strength. This is the case, e.g., of the sulfonic acid resin Amberlyst-15 or the acid zeolites, which present strong Brønsted acid sites leading to low selectivity for the aldol condensation.[54] Therefore, it is demonstrated that these materials have Brønsted acid sites of mild/moderate strength. In addition, an increase in Lewis acid sites population is observed with the incorporation of defects in the structure, leading to a decrease in the ratio of B/L acid sites. Hence, the change in the nature of acid sites, together with the above-mentioned improvement in the accessibility, are the key points to reach high conversion and to keep the high selectivity in the aldol condensation of furfural. The equivalent strong Brønsted acid sites would also promote the oligomerization and polymerization of furfural, leading to a reduced selectivity to the aldol adduct.

Finally, the comparison in morphology of the more active catalyst, UiO-66(Zr)-HCl3, and the non-modulated parent UiO-66(Zr), was determined using TEM. The presence of octahedral UiO-66(Zr) particles with regular crystal faces and relatively uniform size can be observed in the parent material (Fig. 6a and b). However, the use of HCl as modulator during the synthesis seems to lead to a change in morphology, rounding the edges of the octahedral particles (Fig. 6c and d). This can be attributed to the generation of missing-cluster defects in which the whole Zr$_6$ metal cluster is lost from the framework.

In conclusion, it can be stated that the material that has the best catalytic behavior is UiO-66(Zr)-HCl3, obtaining a FAL conversion of 96% and a selectivity to FuMe of 97% in the reaction conditions tested. Similar results are reached over UiO-66(Zr)-HCl4 but with a higher ratio of HCl/ligand during the synthesis.

3.3 Temperature dependence and reaction kinetics study

In order to optimize the process and obtain the kinetic modelling of the reaction over the catalyst selected as optimal, UiO-66(Zr)-HCl3, the influence of reaction temperature on the aldol condensation of FAL and MIBK was studied, varying the temperature in the range 110–170 °C and the reaction time up to 24 h (Fig. 7). At the lowest temperature, the progress of the reaction is very slow, not reaching 100% conversion even after 24 h of reaction. However, working at higher temperatures, a complete conversion of FAL is achieved below 4 h of reaction and the yield of the desired condensation product, FuMe, can reach a maximum around 100%, subsequently decreasing at longer reaction times. This indicates that, as expected at long reaction time or more severe conditions, FuMe undergoes a second condensation reaction with another molecule of MIBK to produce Fu(Me)$_2$ (Scheme 1). Likewise, the formation of degradation compounds is typical of furanic compounds at this range of temperature and in the presence of acid catalysts, so their formation must also be taken into account.

Hence, a plausible reaction pathway for the aldol condensation of FAL and MIBK with the apparent rate constants for each step is shown in Scheme ESI-1.† In the first step one molecule of FAL condense with one molecule of MIBK leading to FuMe, the product of interest (apparent rate constant k_1). Then FuMe may condense with another molecule of MIBK to produce Fu(Me)$_2$, undesirable compound since being a C17 molecule could not be included in the range of aviation fuels. In addition, the formation of other degradation compounds coming from FuMe has been also considered. As neither of these last two transformations is desired, all these products have been included under the term Others (apparent rate constant k_2). The formation of humins from FAL has not been considered in view of the experimental results. The concentration of Others was calculated as the difference between the identified products and the closure of the mass balance. For the two steps described, first order pseudo-homogeneous kinetics have been assumed, being the model equations for the reaction network considered as follows:

$$\frac{\mathrm{d}C_{\text{FAL}}}{\mathrm{d}t} = -k_1 \cdot C_{\text{FAL}}$$

$$\frac{\mathrm{d}C_{\text{FuMe}}}{\mathrm{d}t} = k_1 \cdot C_{\text{FAL}} - k_2 \cdot C_{\text{FuMe}}$$

$$\frac{\mathrm{d}C_{\text{Others}}}{\mathrm{d}t} = k_2 \cdot C_{\text{FuMe}}$$

where C is the molar concentration of reactants and products (mol L^{-1}), and k_i is the apparent rate constant of step i at a constant temperature. It must be noted that catalyst loading has been kept constant in all the experiments, so its influence is not contemplated in the kinetics analysis or in the rate constants. The differential equations system was solved by numerical integration and simultaneous optimization, using the tool Microsoft® Excel SOLVER, by minimizing the objective function defined as the sum of the residual squares:

$$F_{\text{obj}} = \sum_{m} \left\{ \sum_{n=1}^{n_{\text{p}}} \left[C_{m,n,\text{calc}} - C_{m,n,\text{exp}} \right]^2 \right\}$$

where $C_{m,n,\text{calc}}$ and $C_{m,n,\text{exp}}$ are the calculated and experimental concentrations of component m (FAL, FuMe, Others) at a given
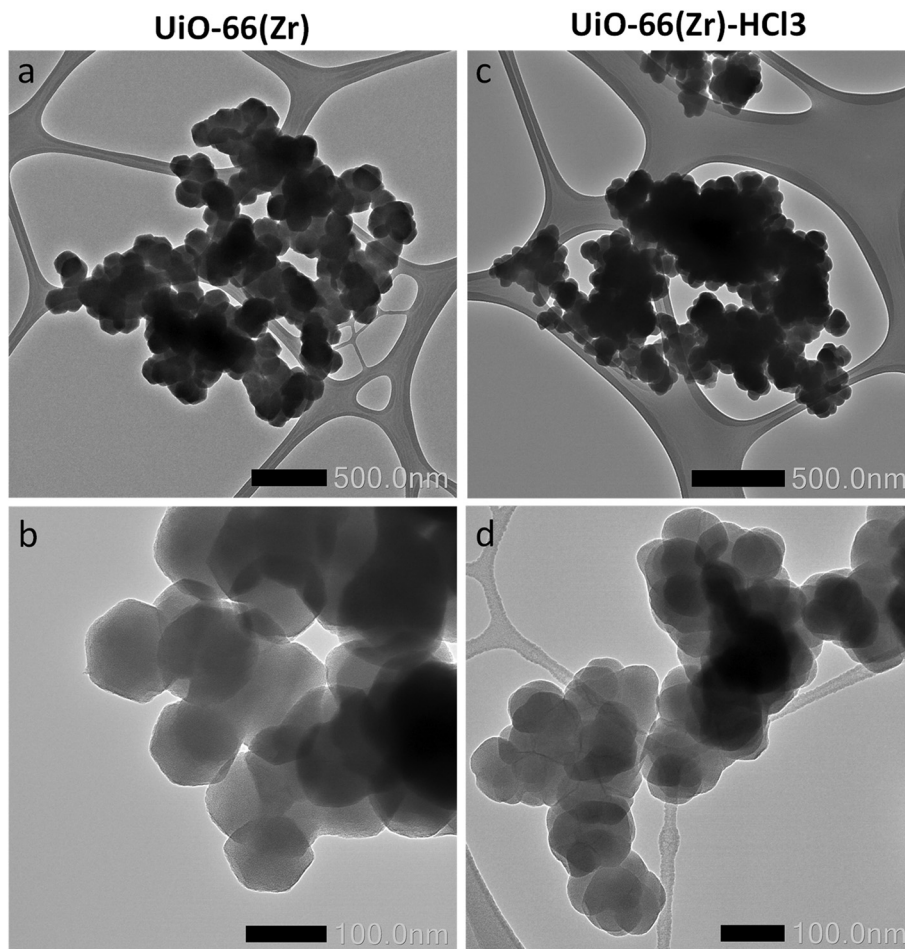
UiO-66(Zr)   UiO-66(Zr)-HCl3

Fig. 6   TEM images of (a and b) UiO-66(Zr) and (c and d) UiO-66(Zr)-HCl3.
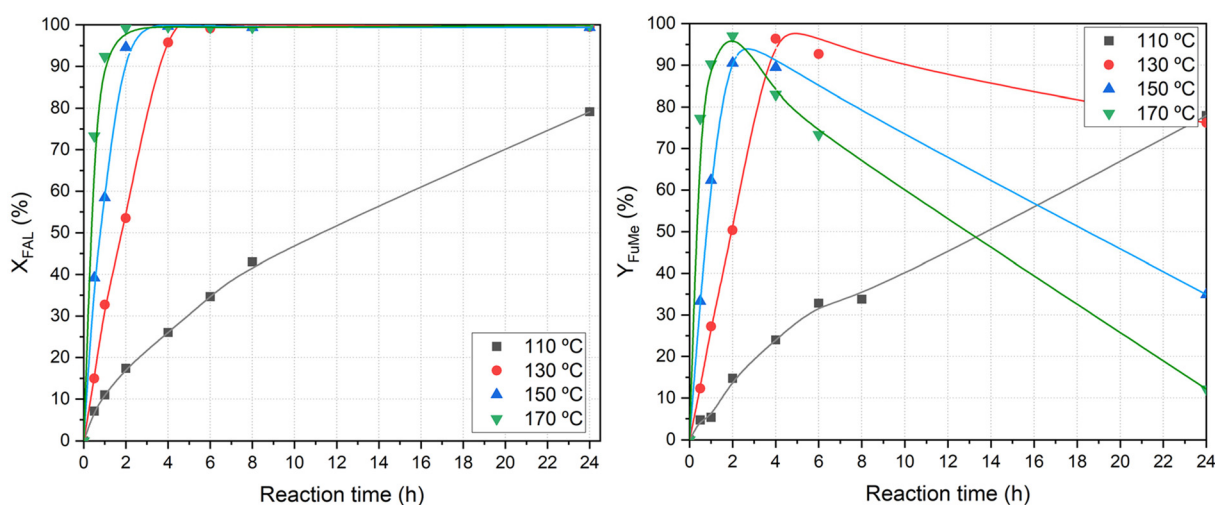

Fig. 7   Influence of temperature on the aldol condensation of FAL and MIBK over UiO-66(Zr)-HCl3. Reaction conditions: MIBK/FAL molar ratio = 4/1; FAL/Cat mass ratio = 10/1.

reaction time n. Table 2 displays the calculated kinetic parameters of the steps involved in the process, including the apparent rate constants (k_i), together with the respective acti-

vation energies (E_a) and pre-exponential factors (k_0), obtained by applying an Arrhenius analysis. The proposed pseudo-first order kinetic model provides a good agreement to the experi-

Table 2 Apparent rate constants (k_i), activation energies (E_a) and pre-exponential factors (k_0) of the modelled aldol condensation of FAL and MIBK over UiO-66(Zr)-HCl3

Reaction step	k_i (h^{-1})				E_a (kJ mol^{-1})	k_0 (h^{-1})	R^2 (Arrhenius)
	110 °C	130 °C	150 °C	170 °C			
1	0.0663	0.4369	0.9788	2.4781	82.9	1.68×10^{10}	0.964
2	0.0000	0.0112	0.0450	0.0650	65.7	4.23×10^{6}	0.915
R^2 (model)	0.996	0.970	0.986	0.991			

mental data (Fig. ESI-6†), indicating a high correlation degree in consonance with the high regression coefficients.

The kinetic constants calculated demonstrate that step 1, the aldol condensation of FAL and MIBK to produce FuMe, is the most favored transformation of the system at all temperatures tested. The formation of Others is negligible at low temperature but at higher temperatures the production of Fu(Me)$_2$ and other by-products begins to be relevant, which leads to a reduction in the yield to the adduct of interest. Therefore, it can be concluded that, working under moderate conditions and with the selected catalyst, it is possible to control the reaction to obtain high FAL conversion and high yield of the desired condensation product.

3.4 Reusability experiments

Finally, the reusability of the optimal catalyst UiO-66(Zr)-HCl3 was assessed by reutilization experiments in three consecutive cycles of aldol condensation reactions under moderate reaction conditions, 130 °C and 3 h. Likewise, two levels of furfural concentration (MIBK/FAL molar ratio = 4 and 8) were evaluated, since in previous studies FAL degradation has been detected as the main potential cause of catalyst deactivation.[54,69] After each run, the catalyst was recovered by filtration, rinsed with acetone at room temperature to remove the reaction media entrapped within the spent catalyst, dried at 110 °C and used in a new reaction run. Fig. 8 shows the catalytic results in terms of FAL conversion and selectivity to FuMe. As shown, at the highest level of furfural concentration (MIBK/FAL = 4) the FAL conversion progressively decreases, although keeping high selectivity around 100%, which evidences a progressive deactivation of the catalyst, most likely by formation of heavy organic deposits coming from FAL degradation. Indeed, the crystallinity of UiO-66(Zr)-HCl3 material is still maintained after 3 consecutive uses in reaction, as determined by XRD (the patterns show very little differences in shape and intensity of reflections compared to the fresh catalyst, Fig. ESI-7†), so the progressive deactivation does not come from any structural deterioration. On the other hand, when working at a lower FAL concentration (MIBK/FAL = 8), this deactivation phenomenon is not observed, at least after three consecutive reaction cycles, maintaining the excellent behavior of the fresh catalyst.
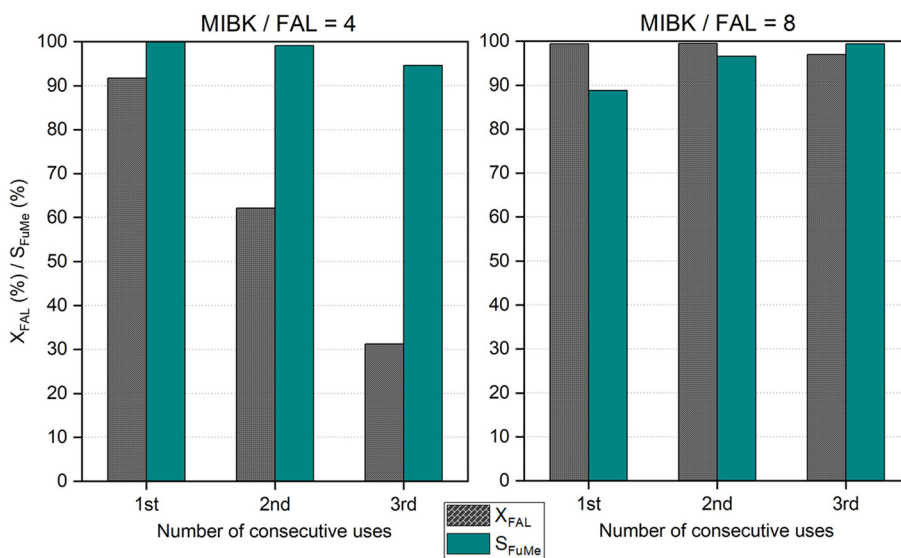

Fig. 8 Reutilization of UiO-66(Zr)-HCl3 in the aldol condensation of FAL and MIBK at two levels of FAL concentration in the reaction medium: MIBK/FAL molar ratio, 4 (left) and 8 (right). Reaction conditions: time = 3 h; temperature = 130 °C; FAL/Cat mass ratio = 10 (left) and FAL/Cat mass ratio = 5 (right).

4. Conclusions

The use of different modulators, such as formic acid, trifluoroacetic acid, and hydrochloric acid, at different concentrations during the synthesis of MOF UiO-66(Zr) incorporates defects into the framework. Thermogravimetric analysis allows for the estimation of the number of linker deficiencies present in the material while Ar adsorption–desorption isotherms is the most appropriate microscopic characterization to verify the existence of missing-cluster defects. The type of modulator used during the synthesis plays an important role in the creation of defects, increasing the number of defects as the pK_a of the modulator decreases. In addition, the type of defect generated is also different: modulators with higher pK_a value, such as formic acid, generate preferentially missing-linker defects while modulators with lower pK_a value, such as HCl, can generate more missing-cluster defects. On the other hand, the catalytic activity of UiO-66(Zr) in the aldol condensation of furfural with MIBK to produce bio jet-fuel precursors can be extraordinarily improved by controlled generation of structural defects in the MOF UiO-66(Zr) by using acid modulators during the synthesis. The creation of missing-linker defects causes the modification of the acid nature of the catalysts, decreasing the Brønsted/Lewis acid sites ratio, while the introduction of missing-clusters defects causes an improvement in the accessibility of those active centers. Therefore, a combination of both types of defects, such as those present in the HCl-modulated Zr-MOF, have shown the best catalytic behaviour in the aldol condensation of FAL and MIBK. Moreover, from the kinetics study it is demonstrated that it is possible to control the reaction to obtain high FAL conversion and selectivity to the desired condensation product, FuMe, working under moderate conditions and with the selected catalyst. Finally, the reusability experiments have shown that when FAL is present in the reaction medium at low concentrations, catalytic performance remains unaltered after three consecutive reaction cycles.

Author contributions

María Sanz: investigation, data curation. Pedro Leo: data curation, methodology, conceptualization. Carlos Palomino: investigation, data curation. Marta Paniagua: conceptualization, writing – original draft preparation, supervision. Gabriel Morales: conceptualization, writing – reviewing and editing, funding acquisition. Juan A. Melero: supervision, writing – reviewing and editing, funding acquisition.

Conflicts of interest

There are no conflicts to declare.

Acknowledgements

References

1 European Commission, *Communication From the Commission to the European Parliament, the Council, the European Economic and Social Committee and the Committee of the Regions: The European Green Deal*, Publications Office of the European Union, 2019.

2 S. S. Doliente, A. Narayan, J. F. D. Tapia, N. J. Samsatli, Y. Zhao and S. Samsatli, *Front. Energy Res.*, 2020, **8**, 110.

3 L. Zhang, L. Tian, R. Sun, C. Liu, Q. Kou and H. Zuo, *Bioresour. Technol.*, 2019, **276**, 60–64.

4 J. Ma, S. Shi, X. Jia, F. Xia, H. Ma, J. Gao and J. Xu, *J. Energy Chem.*, 2019, **36**(9), 74–86.

5 X. Han, Y. Guo, X. Liu, Q. Xia and Y. Wang, *Catal. Today*, 2019, **319**, 2–13.

6 H. Li, A. Riisager, S. Saravanamurugan, A. Pandey, R. S. Sangwan, S. Yang and R. Luque, *ACS Catal.*, 2018, **8**, 148–187.

7 H. Wang, B. Yang, Q. Zhang and W. Zhu, *Renewable Sustainable Energy Rev.*, 2020, **120**, 109612.

8 G. Nie, H. Wang, Q. Li, L. Pan, Y. Liu, Z. Song, X. Zhang, J.-J. Zou and S. Yu, *Appl. Catal., B*, 2021, **292**, 120181.

9 K. Dalvand, J. Rubin, S. Gunukula, M. C. Wheeler and G. Hunt, *Biomass Bioenergy*, 2018, **115**, 56–63.

10 P. Zhou and Z. Zhang, *Catal. Sci. Technol.*, 2016, **6**, 3694–3712.

11 F. Delbecq, Y. Takahashi, T. Kondo, C. C. Corbas, E. R. Ramos and C. Len, *Catal. Commun.*, 2018, **110**, 74–78.

12 R. Mariscal, P. Maireles-Torres, M. Ojeda, I. Sádaba and M. López Granados, *Energy Environ. Sci.*, 2016, **9**, 1144–1189.

13 O. O. James and S. Maity, *Hydrocarbon Biorefinery: Sustainable Processing of Biomass for Hydrocarbon Biofuels*, 2022, pp. 297–325.

14 G. Li, R. Wang, J. Pang, A. Wang, N. Li and T. Zhang, *Chem. Rev.*, 2024, **124**(6), 2889–2954.

15 G. Nie, Y. Dai, Y. Liu, J. Xie, S. Gong, N. Afzal, X. Zhang, L. Pan and J. J. Zou, *Chem. Eng. Sci.*, 2019, **207**, 441–447.

16 X. Zhang, Y. Li, C. Qian, L. An, W. Wang, X. Li, X. Shao and Z. Li, *RSC Adv.*, 2023, **13**, 9466–9478.

17 G. Nie, J. J. Zou, R. Feng, X. Zhang and L. Wang, *Catal. Today*, 2014, **234**, 271–277.

18 Z. Li, Y. Wang and H. Wang, *Energy Technol.*, 2019, **7**, 1900418.

19 G. Li, B. Hou, A. Wang, X. Xin, Y. Cong, X. Wang, N. Li and T. Zhang, *Angew. Chem.*, 2019, **131**, 12282–12286.

20 G. W. Huber, J. N. Chheda, C. J. Barrett and J. A. Dumesic, *Science*, 2005, **308**, 1446–1450.

21 C. J. Barrett, J. N. Chheda, G. W. Huber and J. A. Dumesic, *Appl. Catal., B*, 2006, **66**, 111–118.

22 B. Pholjaroen, N. Li, J. Yang, G. Li, W. Wang, A. Wang, Y. Cong, X. Wang and T. Zhang, *Ind. Eng. Chem. Res.*, 2014, **53**, 13618–13625.

23 J. D. Lewis, S. Van De Vyver and Y. Román-Leshkov, *Angew. Chem., Int. Ed.*, 2015, **54**, 9835–9838.

24 M. Su, W. Li, T. Zhang, H. S. Xin, S. Li, W. Fan and L. Ma, *Catal. Sci. Technol.*, 2017, **7**, 3555–3561.

25 R. M. West, Z. Y. Liu, M. Peter and J. A. Dumesic, *ChemSusChem*, 2008, **1**, 417–424.

26 W. Shen, G. A. Tompsett, K. D. Hammond, R. Xing, F. Dogan, C. P. Grey, W. C. Conner, S. M. Auerbach and G. W. Huber, *Appl. Catal., A*, 2011, **392**, 57–68.

27 H. Olcay, A. V. Subrahmanyam, R. Xing, J. Lajoie, J. A. Dumesic and G. W. Huber, *Energy Environ. Sci.*, 2013, **6**, 205–216.

28 Q. Liu, X. Zhang, Q. Zhang, Q. Liu, C. Wang and L. Ma, *Energy Fuels*, 2020, **34**, 7149–7159.

29 M. Hronec, K. Fulajtárova, T. Liptaj, M. Štolcová, N. Prónayová and T. Soták, *Biomass Bioenergy*, 2014, **63**, 291–299.

30 Q. Liu, C. Zhang, N. Shi, X. Zhang, C. Wang and L. Ma, *RSC Adv.*, 2018, **8**, 13686–13696.

31 J. Yang, N. Li, G. Li, W. Wang, A. Wang, X. Wang, Y. Cong and T. Zhang, *ChemSusChem*, 2013, **6**, 1149–1152.

32 W. Wang, X. Ji, H. Ge, Z. Li, G. Tian, X. Shao and Q. Zhang, *RSC Adv.*, 2017, **7**, 16901–16907.

33 J. Cueto, L. Faba, E. Díaz and S. Ordóñez, *Appl. Catal., B*, 2020, **263**, 118341.

34 M. C. Hernández-Soto, A. Erigoni, C. Segarra, F. Rey, U. Díaz, E. Gianotti, I. Miletto and M. Pera-Titus, *Appl. Catal., A*, 2022, **643**, 118710.

35 Y. Zhao, M. Fan, P. Wang, C. Li, L. Wang and L. Wang, *Fuel Process. Technol.*, 2020, **198**, 106250.

36 X. Kong, X. Wei, L. Li, Z. Fang and H. Lei, *Catal. Commun.*, 2021, **149**, 106207.

37 A. Bavykina, N. Kolobov, I. S. Khan, J. A. Bau, A. Ramirez and J. Gascon, *Chem. Rev.*, 2020, **120**, 8468–8535.

38 L. Zhu, X. Q. Liu, H. L. Jiang and L. B. Sun, *Chem. Rev.*, 2017, **117**, 8129–8176.

39 A. Herbst and C. Janiak, *CrystEngComm*, 2017, **19**, 4092–4117.

40 R. Fang, A. Dhakshinamoorthy, Y. Li and H. Garcia, *Chem. Soc. Rev.*, 2020, **49**, 3638–3687.

41 J. H. Cavka, S. Jakobsen, U. Olsbye, N. Guillou, C. Lamberti, S. Bordiga and K. P. Lillerud, *J. Am. Chem. Soc.*, 2008, **130**, 13850–13851.

42 H. Wu, T. Yildirim and W. Zhou, *J. Phys. Chem. Lett.*, 2013, **4**, 925–930.

43 J. Winarta, B. Shan, S. M. McIntyre, L. Ye, C. Wang, J. Liu and B. Mu, *Cryst. Growth Des.*, 2020, **20**, 1347–1362.

44 Y. Feng, Q. Chen, M. Jiang and J. Yao, *Ind. Eng. Chem. Res.*, 2019, **58**, 17646–17659.

45 G. C. Shearer, S. Chavan, J. Ethiraj, J. G. Vitillo, S. Svelle, U. Olsbye, C. Lamberti, S. Bordiga and K. P. Lillerud, *Chem. Mater.*, 2014, **26**, 4068–4071.

46 G. Ye, D. Zhang, X. Li, K. Leng, W. Zhang, J. Ma, Y. Sun, W. Xu and S. Ma, *ACS Appl. Mater. Interfaces*, 2017, **9**, 34937–34943.

47 F. Vermoortele, B. Bueken, G. Le Bars, B. Van De Voorde, M. Vandichel, K. Houthoofd, A. Vimont, M. Daturi, M. Waroquier, V. Van Speybroeck, C. Kirschhock and D. E. De Vos, *J. Am. Chem. Soc.*, 2013, **135**, 11465–11468.

48 B. Bueken, N. Van Velthoven, A. Krajnc, S. Smolders, F. Taulelle, C. Mellot-Draznieks, G. Mali, T. D. Bennett and D. De Vos, *Chem. Mater.*, 2017, **29**, 10478–10486.

49 Z. Niu, Q. Guan, Y. Shi, Y. Chen, Q. Chen, Z. Kong, P. Ning, S. Tian and R. Miao, *New J. Chem.*, 2018, **42**, 19764–19770.

50 O. V. Gutov, M. G. Hevia, E. C. Escudero-Adán and A. Shafir, *Inorg. Chem.*, 2015, **54**, 8396–8400.

51 L. Zhou, X. Zhang and Y. Chen, *Mater. Lett.*, 2017, **197**, 167–170.

52 S. Yuan, J. S. Qin, C. T. Lollar and H. C. Zhou, *ACS Cent. Sci.*, 2018, **4**, 440–450.

53 A. Bavykina, N. Kolobov, I. S. Khan, J. A. Bau, A. Ramirez and J. Gascon, *Chem. Rev.*, 2020, **120**, 8468–8535.

54 D. de la Flor, C. López-Aguado, M. Paniagua, G. Morales, R. Mariscal and J. A. Melero, *J. Catal.*, 2021, **401**, 27–39.

55 S. Feng, X. Zhang, Q. Zhang, Y. Liang, X. Zhao, C. Wang and L. Ma, *Fuel*, 2021, **299**, 120889.

56 G. C. Shearer, S. Chavan, J. Ethiraj, J. G. Vitillo, S. Svelle, U. Olsbye, C. Lamberti, S. Bordiga and K. P. Lillerud, *Chem. Mater.*, 2014, **26**, 4068–4071.

57 M. J. Cliffe, W. Wan, X. Zou, P. A. Chater, A. K. Kleppe, M. G. Tucker, H. Wilhelm, N. P. Funnell, F. X. Coudert and A. L. Goodwin, *Nat. Commun.*, 2014, **5**, 1–8.

58 J. Winarta, B. Shan, S. M. McIntyre, L. Ye, C. Wang, J. Liu and B. Mu, *Cryst. Growth Des.*, 2020, **20**, 1347–1362.

59 G. C. Shearer, S. Chavan, S. Bordiga, S. Svelle, U. Olsbye and K. P. Lillerud, *Chem. Mater.*, 2016, **28**, 3749–3761.

60 M. J. Katz, Z. J. Brown, Y. J. Colón, P. W. Siu, K. A. Scheidt, R. Q. Snurr, J. T. Hupp and O. K. Farha, *Chem. Commun.*, 2013, **49**, 9449–9451.

61 F. Vermoortele, B. Bueken, G. Le Bars, B. Van De Voorde, M. Vandichel, K. Houthoofd, A. Vimont, M. Daturi, M. Waroquier, V. Van Speybroeck, C. Kirschhock and D. E. De Vos, *J. Am. Chem. Soc.*, 2013, **135**, 11465–11468.

62 B. Shan, S. M. McIntyre, M. R. Armstrong, Y. Shen and B. Mu, *Ind. Eng. Chem. Res.*, 2018, **57**, 14233–14241.

63 L. Liu, Z. Chen, J. Wang, D. Zhang, Y. Zhu, S. Ling, K. W. Huang, Y. Belmabkhout, K. Adil, Y. Zhang, B. Slater, M. Eddaoudi and Y. Han, *Nat. Chem.*, 2019, **11**, 622–628.

64 G. C. Shearer, S. Chavan, J. Ethiraj, J. G. Vitillo, S. Svelle, U. Olsbye, C. Lamberti, S. Bordiga and K. P. Lillerud, *Chem. Mater.*, 2014, **26**, 4068–4071.

65 T. Yang, Y. Gao, Q. He, Y. Chai, P. Qin, Z. Wu, C. Liu, X. Gong and Y. Liang, *Chem. Eng. J.*, 2024, **486**, 149971.

66 K. Chakarova, I. Strauss, M. Mihaylov, N. Drenchev and
    K. Hadjiivanov, *Microporous Mesoporous Mater.*, 2019, **281**,
    110–122.

67 S. Rojas-Buzo, B. Bohigues, C. W. Lopes, M. Meira,
    M. Boronat, M. Moliner and A. Corma, *Chem. Sci.*, 2021, **12**,
    10106–10115.

68 R. C. Klet, Y. Liu, T. C. Wang, J. T. Hupp and O. K. Farha,
    J. Mater. Chem. A, 2016, **4**, 1479–1485.

69 G. Morales, M. Paniagua, D. de la Flor, M. Sanz,
    P. Leo, C. López-Aguado, H. Hernando, S. A. Orr,
    K. Wilson, A. F. Lee and J. A. Melero, *Fuel*, 2023, **339**,
    127465.